

High T_C ferromagnetic inverse Heusler alloys: A comparative study of Fe_2RhSi and Fe_2RhGe

Y. Venkateswara,¹ S. Shanmukharao Samatham,^{1,2} Akhilesh Kumar Patel,¹
P. D. Babu,³ Manoj Raama Varma,⁴ K. G. Suresh,^{1,*} and Aftab Alam^{5,†}

¹Magnetic Materials Laboratory, Department of Physics,

Indian Institute of Technology Bombay, Mumbai 400076, India

²Department of Physics, Maharaj Vijayaram Gajapathi Raj College of Engineering,

Vijayaram Nagar Campus, Chintalavalasa, Vizianagaram 535005, Andhra Pradesh, India

³UGC-DAE Consortium for Scientific Research, Mumbai Centre, BARC Campus, Mumbai 400085, India

⁴National Institute of Interdisciplinary Sciences and Technology (CSIR), Tiruvananthapuram, India

⁵Materials Modeling Laboratory, Department of Physics,

Indian Institute of Technology Bombay, Mumbai 400076, India

(Dated: December 3, 2021)

We report the results of experimental investigations on structural, magnetic, resistivity, caloric properties of Fe_2RhZ ($Z=\text{Si, Ge}$) along with *ab-initio* band structure calculations using first principle simulations. Both these alloys are found to crystallize in inverse Heusler structure but with disorder in tetrahedral sites between Fe and Rh. Fe_2RhSi has saturation moment of $5.00 \mu_B$ and while its counterpart has $5.19 \mu_B$. Resistivity measurement reveals metallic nature in both of them. Theoretical simulations using generalized gradient approximation (GGA) predict inverse Heusler structure with ferromagnetic ordering as ground state for both the alloys. However it underestimates the experimentally observed moments. GGA+ U approach, with Hubbard U values estimated from density functional perturbation theory helps to improve the comparison of the experimental results. Fe_2RhSi is found to be half metallic ferromagnet while Fe_2RhGe is not. Varying U values on Fe and Rh sites does not change the net moment much in Fe_2RhSi , unlike in Fe_2RhGe . Relatively small exchange splitting of orbitals in Fe_2RhGe compared to that of Fe_2RhSi is the reason for not opening the band gap in the minority spin channel in the former. High ordering temperature and moment make Fe_2RhSi useful for spintronics applications.

PACS numbers: 75.50.Bb, 75.47.Np, 61.10.Nz, 61.66.Dk, 72.25.Ba, 85.75.-d, 75.76.+j, 76.80.+y

I. INTRODUCTION

Heusler alloys (HAs)¹ are well known due to their multifunctional properties such as (i) half metallic ferromagnetism,^{2,3} spin gapless semiconducting nature,⁴⁻⁶ bipolar magnetic semiconductors⁷ and spin semimetals,⁸ (ii) high spin polarization (iii) superconductivity arising in the alloys containing 27 valence electrons such as Ni_2ZrGa ,⁹ Pd_2RSn ($R=\text{Tb-Yb}$)¹⁰⁻¹², AuPdTM ($T=\text{Sc, Y}$ and $M=\text{Al, Ga, In}$)¹³ etc., (iv) giant exchange bias,^{14,15} (v) Martensitic transition which causes large magneto-caloric effect (MCE)¹⁶⁻¹⁸ and topological insulating behaviour¹⁹⁻²⁵ and Weyl semimetals.^{26,27} For the last three decades, after discovery of half-metallicity in NiMnSb by de Groot *et. al.*,² HAs gained prominence in the field of spintronics. Among the studied systems, Co-based Heusler alloys got increased attention due to their high Curie temperature (T_C). In addition to the $3d$ based HAs, $4d$ based alloys were also studied for spintronic applications. Some of the examples are $\text{Ru}_{2-x}\text{Fe}_x\text{CrGe}$,²⁸ $\text{Ru}_{2-x}\text{Fe}_x\text{CrSi}$,²⁹ Ru_2MnZ ($Z=\text{Si, Ge, Sn}$ and Sb),³⁰ $(\text{Ru}_{1-x}\text{Co}_x)_2\text{FeSi}$,³¹ RuMn_2Z ($Z=\text{Si, Sn}$)³² and CoFeRuZ ($Z=\text{Si, Ge}$)³³. In these alloys, Ru couples antiferromagnetically with neighboring magnetic ions. The other important high T_C series of $4d$ based Heusler alloys are Rh based. There has been extensive effort in the synthesis of the class of Rh_2TX ($T=\text{Ti, V, Cr, Mn, Fe, Co, Ni, Cu; X=Al, Ga, Ge, Si, Sb, Pb}$) alloys.³⁴⁻⁴⁰ However, L_{21} order is found only for $T=\text{Mn, Ni}$ and Cu . Others either show tetragonal distortion or involve multiphases. Interestingly, in almost all studies in the literature on Rh-based HAs, researchers have achieved the ordered L_{21} structure only if the total number of valence electrons of the alloy is odd. Some of the examples include Rh_2MnX ($X=\text{Ge, Sn, Pb}$),³⁴ Rh_2CuSn ,^{36,41,42} LiRh_2X ($X=\text{Si, Ge}$),⁴³ CoRhMnSn ,⁴⁴ CoRhMnGe ,⁴⁵ FeRhCrGe ⁸ etc. Even though Rh_2NiGe is reported to crystallize in L_{21} structure, one can notice extra impurity peaks in the reported XRD data.³⁸

Rh-based Heusler alloys, with even number of valence electrons show tetragonal distortion which can be explained using band Jahn-Teller effect.⁴⁶ For these alloys, Coulomb repulsion also plays a crucial role in separating out the electronic states by broadening of the energy bands (close to the Fermi level), resulting in lattice distortion. One exception is the set of alloys containing Mn, such as CoRhMnGa ,⁴⁴ as Mn has the ability to adopt different oxidation states. Another reason is the nature of hybridization of Mn-atom with different neighboring orbitals as can be noticed in CoRuMnSi ⁴⁷, unlike the general hybridization followed in other HAs reported elsewhere.^{48,49} See supplementary material⁸ for more details.

In this paper, we report two new odd-valence elec-

tron Rh-based full Heusler alloys Fe_2RhZ ($Z=\text{Si, Ge}$). A detailed experimental investigation involving structural, magnetic and transport behavior is carried out. Additionally, first principle calculations are done to better understand the magnetic ordering and the electronic structure.

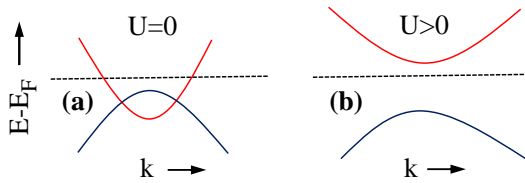


FIG. 1. Atom projected orbital character of bands close to Fermi level. (Left) Direct overlap of orbitals in the absence of Hubbard (U) correction, (right) gapped orbitals due to the inclusion of Hubbard correction. Partially occupied orbital (red color) corresponds to octahedral site while valence orbital (blue color) corresponds to tetrahedral sites in Heusler alloy.

Fe_2RhZ ($Z=\text{Si, Ge}$) are 29 valence electrons Heusler systems and hence are the analogue of $3d$ -based Heusler alloys such as Fe_2CoSi ,⁵⁰ Fe_2CoGe ,^{51,52} Co_2FeSi ,^{53–56} Co_2FeGe ^{57–60} etc. Wurmehl *et. al.*^{54,56} and Uvarov *et. al.*^{58,59} studied Co_2FeSi and Co_2FeGe respectively and reported that they could only produce the experimentally observed moment and gap in the minority band by applying Hubbard U on these systems. But they have neither discussed why they have to include Hubbard U in their systems nor gave a clear indication to what type of Heusler systems it should be included. There is an ambiguity of inclusion of U in all Heusler systems. Here we present a systematic way to observe and identify which Heusler systems need to be taken care with the inclusion of Hubbard correction. Figure 1(a) represents the atom resolved orbital character of band structure without Hubbard correction. If one notices such a direct overlap of orbitals (or slightly gapped) typically around the edges of the Brillouin zone (or away from the Γ point), they need to identify the atomic orbital character of these bands. (One can recall that the orbitals at Γ represent molecular levels of the corresponding system). If the partially occupied conduction band (indicated by red color in Fig.1(a)) arises from the octahedral site while the valence band arises from the tetrahedral site, then one should not neglect the Hubbard correction in the Heusler system. This kind of scenario generally occurs in high valence systems in the spin down band around X -point in the Brillouin zone. As per the empirical rule stated in Ref.[61] for the formation of Heusler alloys based on electronegativities of constituent atoms, the octahedral sites try to lose partial electrons. Hence, the partially occupied conduction band which corresponds to octahedral site lose their states by shifting their orbitals above the Fermi level. Such an observation can only be achieved by the inclusion of U in the system as shown in Fig.1(b). Because U correction favours integer particle numbers in the system by penalizing the partial occupancies. Therefore one should look

for such direct overlap of orbitals (i) in minority band for ferro, ferri- or fully compensated ferri- magnets or (ii) in the full band structure for anti-ferromagnets or non-magnetic systems. The effect of U is to open up the gap around the k -point in the Brillouin zone but does not always guarantee in the entire Brillouin zone as shown for Fe_2RhGe later in this paper. With this methodology one can predict very accurate results prior to experimental observations.

Theoretically, full Heusler alloys can accommodate a maximum of 31 valence electrons and can have a moment close to $7 \mu_B$. This happens only when the spin up bands are completely filled with integral number of electrons. Experimentally, all such high valence electron systems reported in the literature belong to 29 and 30 valence electrons category. Fe_2RhZ ($Z=\text{Si, Ge}$) are the two new systems belonging to this category, with reasonably large T_C and magnetic moment.

II. EXPERIMENTAL TECHNIQUES

Both Fe_2RhSi and Fe_2RhGe alloys were prepared in polycrystalline form by arc-melting method. Room temperature X-ray diffraction (XRD) patterns were collected by PANalytical X'Pert Pro powder diffractometer using $\text{Cu K}\alpha$ radiation. Rietveld refinement of XRD patterns were analyzed using FullProf⁶² package while VESTA⁶³ software is used for visualizing crystal structures. Magnetization measurements were carried out using Physical Property Measurement System (PPMS) model 6000 within the vibrating sample magnetometer (VSM) option. Resistivity measurements were carried out using PPMS at different magnetic fields. Specific heat measurements were carried out from 2 to 280 K at zero field in PPMS using relaxation calorimetry.

III. COMPUTATIONAL DETAILS

Fe_2RhZ ($Z=\text{Si, Ge}$) with the stoichiometry 2:1:1 belong to the full Heusler alloy family. There exist two non-degenerate crystal configurations/structures in this class: i) inverse Heusler structure (X type structure with prototype CuHg_2Ti , space group $F\bar{4}3m$) and ii) normal Heusler structure ($L2_1$ structure with prototype Cu_2MnAl , space group $Fm\bar{3}m$) which are shown in Figs. 2(a) and 2(b) respectively. Since the valence of Fe is less than that of Rh, these alloys are expected to crystallize in inverse Heusler structure. It originates from the simple empirical rule.⁴⁸ In a full $\text{HA } X_2YZ$, keeping Z at 4a site (i.e. at $(0,0,0)$), the lattice sites involving Fe and Rh atoms can have the following two configurations:

- I. Fe1 at $4b(\frac{1}{2}, \frac{1}{2}, \frac{1}{2})$, Fe2 at $4c(\frac{1}{4}, \frac{1}{4}, \frac{1}{4})$ and Rh at $4d(\frac{3}{4}, \frac{3}{4}, \frac{3}{4})$,
- II. Rh at $4b(\frac{1}{2}, \frac{1}{2}, \frac{1}{2})$ and Fe's at $4c(\frac{1}{4}, \frac{1}{4}, \frac{1}{4})$ and $4d(\frac{3}{4}, \frac{3}{4}, \frac{3}{4})$.

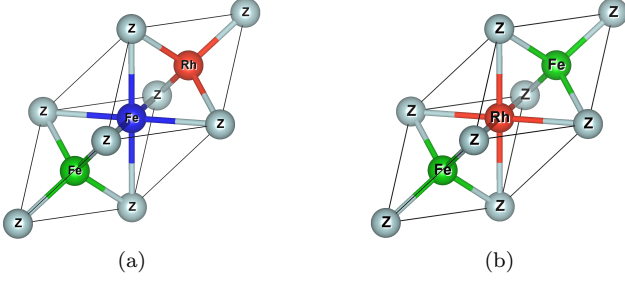


FIG. 2. Possible crystallographic configurations for Fe_2RhZ ($Z = \text{Si}, \text{Ge}$) full HAs. (a) Inverse Heusler structure (configuration I) and (b) normal Heusler structure (configuration II).

We used Quantum ESPRESSO^{64,65} to simulate the two systems with different initial structural and spin configurations on Fe and Rh ions, and find the most stable (ground) state. Exchange correlations are incorporated within the generalized gradient approximation (GGA) and the pseudopotentials parameterized by plane augmented wave method (KJPAW)⁶⁶ were generated using PSLibrary⁶⁷. Other computational parameters used here are the same as in our previous report.⁶⁸ We used XCrySDen for making k -point path for band structure calculations.⁶⁹

IV. EXPERIMENTAL RESULTS

A. Crystal structure

Figures 3(a) and 3(c) show the room temperature XRD pattern along with their Rietveld refinement for Fe_2RhSi and Fe_2RhGe respectively. The XRD pattern can be indexed with CuHg_2Ti type inverse Heusler structure with lattice parameters 5.77 Å and 5.88 Å for the two alloys respectively. However, the observed peak intensity is weaker than that calculated for the odd superlattice reflections such as (111), (311) *etc.* indicating disorder between either tetrahedral site or octahedral site atoms. Octahedral disorder between Fe and Z(Si,Ge) does not fit well whereas 50% disorder of tetrahedral site atoms Fe and Rh in configuration I fits very well (see the zoomed-in view of Figs. 3(a) and 3(c)). Figures 3(b) and 3(d) show the primitive cells corresponding to the best fit. Refinement does not fit well for both odd and even superlattice reflection peaks in configuration II (Cu_2MnAl type structure). Moreover, any amount of disorder such as (i) $L2_1$ disorder between either octahedral or tetrahedral sites, (ii) DO_3 disorder, (iii) B2 disorder and (iv) A2 disorder also did not fit well for configuration II. Hence, we conclude that both the alloys crystallize in inverse Heusler structure with 50% disorder between tetrahedral site atoms Fe and Rh.

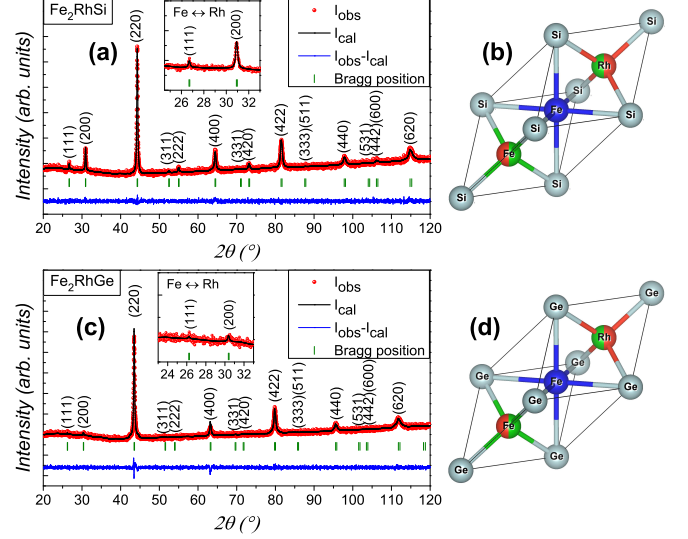


FIG. 3. Rietveld refinement of room temperature XRD data for (top) Fe_2RhSi and (bottom) Fe_2RhGe respectively. Inset of (a) and (c) show the zoomed-in view of the refined data considering disorder between Fe and Rh in inverse Heusler structure (best fit). (b) and (d) Primitive cells corresponding to the best fit in (a) and (c) respectively.

B. Magnetization

The magnetization (M) in full Heusler alloys can be roughly estimated using the Slater-Pauling (SP) rule,⁴⁹ given below

$$M = (N_v - 24) \mu_B/f.u., \quad (1)$$

where N_v is the total number of valence electrons in the alloy. Since both the alloys have 29 valence electrons, they are expected to have a saturation moment of 5 $\mu_B/f.u.$, as per SP rule.

Both the alloys are found to be ferromagnetic in nature with high Curie temperatures. Magnetization vs. field data at 3 K and 300 K are shown in Figs. 4(a) and 4(c) for Fe_2RhSi and Fe_2RhGe respectively. Fe_2RhSi has saturation moment of 5 $\mu_B/f.u.$, whereas Fe_2RhGe has 5.19 $\mu_B/f.u.$, which are consistent with the SP rule. Nearly integer moment on Fe_2RhSi indicates the possibility of half-metallic nature. Figure 4(b) and 4(d) show the temperature dependence of magnetization for the two alloys at 500 Oe. We have also performed high T magnetization measurements up to 1000 K which confirm the T_C for Fe_2RhSi and Fe_2RhGe to be 925 K and 910 K respectively.

C. Resistivity

Figure 5 shows the temperature dependence of resistivity for Fe_2RhSi and Fe_2RhGe , measured in the range 2-350 K. Measurements were carried out at different mag-

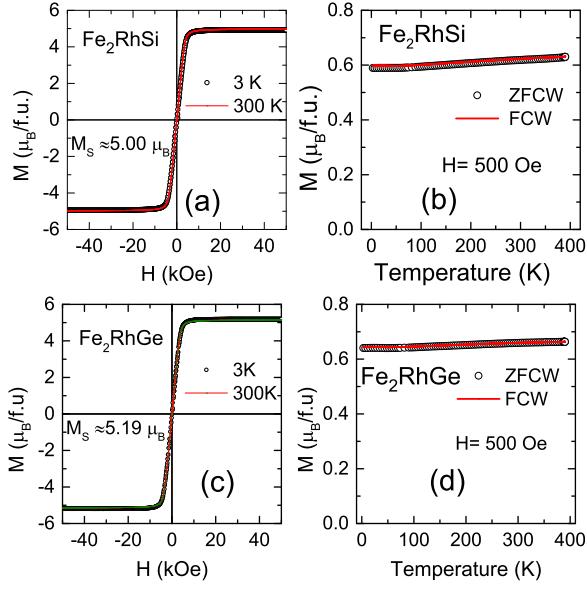


FIG. 4. (a) Magnetization vs. field (H) at 3 K and 300 K for (a) Fe_2RhSi and (c) Fe_2RhGe . Magnetization vs. temperature (T) at 500 Oe for (b) Fe_2RhSi and (d) Fe_2RhGe .

netic fields 0, 5, 10 and 50 kOe. In zero field, the positive temperature coefficient of $\rho(T)$ indicates metallic behavior. The application of field does not change the resistivity behavior much, as evident from Fig. 5(a), thereby indicating the robust magnetic ordering of the alloys. The absence of positive magnetoresistance indicates the marginal effect of field on the motion of conduction electrons. Resistivity data is fitted with the relation $\rho = \rho_0 + AT^n$ where ρ_0 is the residual resistivity. The residual resistance ratio ($RRR = R_{300K}/R_{2K}$) of Fe_2RhSi and Fe_2RhGe is ≈ 1.6 . Such of a low RRR, as compared to that of conventional metals, is typical to Heusler alloys. Figures 5(b) and 5(c) show the fitted curve in two temperature regions (2-75 K and 50-350 K) with almost equal residual resistivity values. In the low T -region, the exponents turn out to be ~ 2.99 and ~ 2.83 for Fe_2RhSi and Fe_2RhGe respectively while they are $n \sim 1.54$ and ~ 1.59 in the high T -range. Fu-

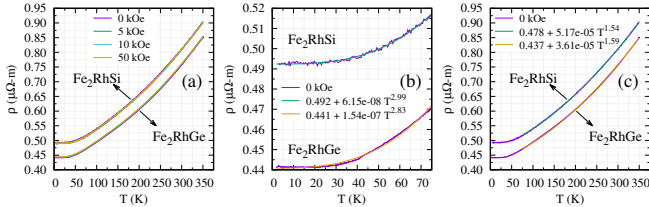


FIG. 5. (Color online) (a) Temperature(T) dependence of resistivity (ρ) at different magnetic fields for Fe_2RhSi and Fe_2RhGe . (b) Low T and (c) high T exponent fit ($\rho(T) = \rho_0 + AT^n$) to the resistivity data for Fe_2RhSi and Fe_2RhGe .

rukawa derived the expression $\rho \propto (T/D_s)^3$ for the possible anomalous single magnon scattering at low temperatures in half metals.⁷⁰ The same behavior is also observed in half metallic systems $\text{Sm}_{0.6}\text{Sr}_{0.4}\text{MnO}_3$ and $(\text{Nd}_{0.8}\text{Tb}_{0.2})_{0.6}\text{Sr}_{0.4}\text{MnO}_3$.⁷¹ Hence the T^3 dependence observed in Fe_2RhSi at low temperatures indicates the half metallic nature whereas the exponent for Fe_2RhGe is slightly off from cubic dependence. The exponent in the high T fitting, however is close to $5/3$, indicating the presence of high temperature spin waves.^{72,73}

D. Specific heat

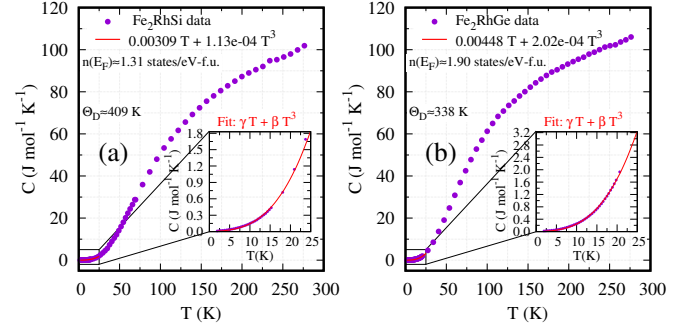


FIG. 6. Specific heat(C) vs. T for (a) Fe_2RhSi and (b) Fe_2RhGe between 2-280 K in zero field. Insets show the zoomed in view of the low temperature fit, $C(T) = \gamma T + \beta T^3$ in the T -range 2-22 K.

Figure 6(a) and 6(b) show the temperature dependence of zero field specific heat (C) for Fe_2RhSi and Fe_2RhGe respectively. The low temperature specific heat is fitted to the expression $C(T) = \gamma T + \beta T^3$ from 2-22 K, as shown in insets of Figs. 6(a) and 6(b) respectively. Here γT and βT^3 are electronic and low temperature phonon contributions. The density of states (DOS) at the Fermi level $n(E_F)$ responsible for electronic contribution is estimated using the relation $n(E_F) = 3\gamma/(\pi k_B)^2$,⁷⁴ where γ is Sommerfeld constant obtained from the fit and k_B is Boltzmann constant. The Debye temperature Θ_D is estimated using the relation $\Theta_D = \sqrt[3]{1944p/\beta}$, where β is the coefficient of T^3 dependence at low temperatures and p is the number of atoms in a formula unit. The values of γ and β in units of $\text{mJ mol}^{-1} \text{K}^{-2}$ and $\text{J mol}^{-1} \text{K}^{-4}$ are estimated to be 3.09 ± 0.33 and $(1.13 \pm 0.01) \times 10^{-4}$ for Fe_2RhSi and 4.48 ± 0.49 , $(2.02 \pm 0.02) \times 10^{-4}$ for Fe_2RhGe . Thus estimated $n(E_F)$ are 1.31 ± 0.13 states/eV-f.u. and 1.90 ± 0.21 states/eV-f.u. for Fe_2RhSi and Fe_2RhGe respectively. The estimated Θ_D are 409 K and 338 K for Fe_2RhSi and Fe_2RhGe respectively. The estimated $n(E_F)$ values are in good agreement with the simulated results using GGA+ U approach. It predicts nearly 1.0 states/eV-f.u. and 1.9 states/eV-f.u. for Fe_2RhSi and Fe_2RhGe respectively. The values of C slightly larger than $100 \text{ J mol}^{-1} \text{K}^{-1}$ (Dulong-petit law) for $T > 250$ K

TABLE I. Relaxed lattice parameter (a_0), atom projected moments and total cell moment, relative energy (ΔE) of different configurations of Fe_2RhZ ($Z=\text{Si, Ge}$) within GGA functional.

Config.	Alloy	a_0 (Å)	Moment (μ_B)				ΔE (meV/atom)
			4d	4b	4c	Total	
			Fe1	Fe2	Rh		
I	Fe_2RhSi	5.79	1.70	2.80	0.40	4.90	0.0
	Fe_2RhGe	5.90	1.84	2.84	0.35	5.03	0.0
II	Fe_2RhSi	5.80	1.89	0.60	1.89	4.38	282
	Fe_2RhGe	5.91	2.10	0.62	2.10	4.92	235

indicate the presence of small but non-negligible magnon contribution to specific heat.

V. THEORETICAL RESULTS AND DISCUSSION

Both Fe_2RhSi and Fe_2RhGe alloys were fully relaxed in the two configurations I and II using GGA functional. The magnetic state and their total energies at the relaxed lattice parameters (a_0) are listed in Table I. Configuration I is found to be energetically, more stable indicating that the alloys prefer inverse Heusler structure. The calculated net magnetic moments for Fe_2RhSi and Fe_2RhGe are $4.90 \mu_B$ and $5.03 \mu_B$ respectively which are in fair agreement with SP rule and the experimental values.

Figure 7 shows the spin resolved band structure and density of states for configuration I of Fe_2RhZ ($Z=\text{Si}$ and Ge) using GGA functional. The band structure clearly

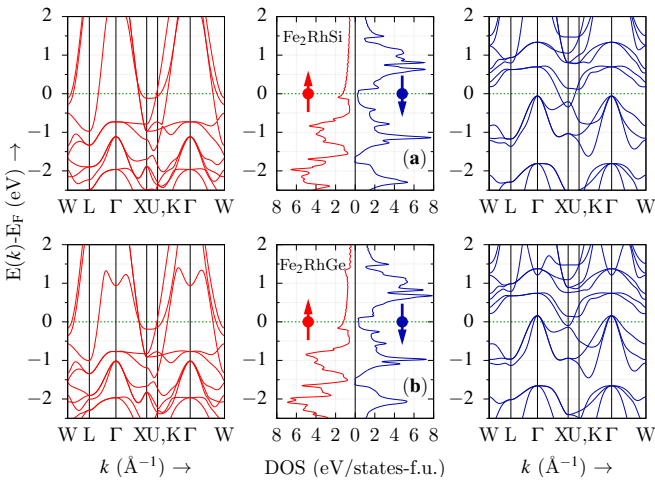


FIG. 7. Spin resolved band structure and density of states for configuration I of (top) Fe_2RhSi and (bottom) Fe_2RhGe at their equilibrium lattice parameter(a_0) within GGA functional.

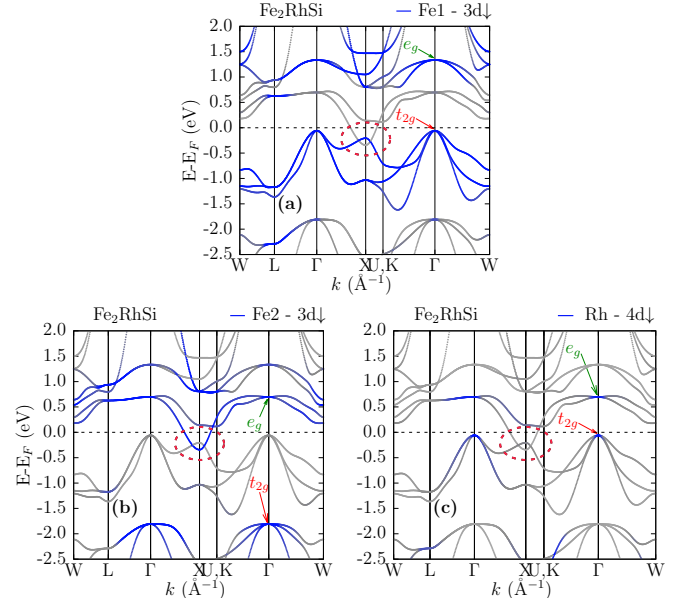


FIG. 8. d orbital projected band structure of spin down channel for configuration I of Fe_2RhSi with GGA functional. (a) $3d$ orbital character of tetrahedral site atom Fe, (b) $3d$ orbital character of octahedral site atom Fe and (c) $4d$ orbital character of another tetrahedral site atom Rh.

indicates that neither of the two systems is half metallic due to presence of small finite DOS at E_F in the spin down band. The small DOS arises due to the overlap of pair of valence and conduction bands around X point in Brillouin zone. The character of these bands is obtained by projecting atomic orbitals on different atomic sites, as shown in Fig. 8 for Fe_2RhSi . One can notice from Figs. 8(a)-(c) that the conduction orbital is mainly contributed by e_g character of octahedral site Fe (denoted as Fe2) while valence orbital by t_{2g} character of tetrahedral site Fe (denoted as Fe1) around the X -point, as highlighted by dotted encircle. This depicts the Hubbard picture as these orbitals are arising from different sites, but by the same atom (i.e. Fe) and are overlapping with same moment and energy due to direct overlap. This leaves the possibility of exchange of indistinguishable particles between two distinct sites of Fe. A similar scenario can be noticed in the band structure of Fe_2RhGe using GGA functional (please see supplement⁷⁵). Hence, we decided to carry out the simulations using GGA+ U functional. This is carried out in two ways, (i) self consistent evaluation of U values on Hubbard atoms, i.e. Fe1, Fe2 and Rh, unlike trial and error method, (ii) step wise increment of U on Hubbard atoms.

Self consistent estimation of U values on different atomic sites (Fe1, Fe2 and Rh) in both the configurations of Fe_2RhSi and Fe_2RhGe is carried out using linear response method as described by Coccioni *et. al.*⁷⁶ Please see supplementary material⁷⁵ for details on deriving U values at different Hubbard sites. U values are estimated with increasing supercell size and the converged values

TABLE II. Self consistently converged Hubbard energies(U) on Fe1, Fe2 and Rh atoms for the two configurations (I and II) of Fe_2RhZ ($\text{Z}=\text{Si}, \text{Ge}$).

Config.	Alloy	Hubbard U (eV)		
		4d	4b	4c
I		Fe1	Fe2	Rh
	Fe_2RhSi	5.2	4.1	6.8
	Fe_2RhGe	4.6	3.9	6.6
II		Fe1	Rh	Fe2
	Fe_2RhSi	3.8	5.3	3.8
	Fe_2RhGe	3.5	5.2	3.5

are taken for the final GGA+ U calculations.

Table II shows the converged Hubbard U energies on different atoms for both the configurations of the two systems. One can notice the different U values on Fe1 and Fe2 due to their different chemical environments with $U_{\text{Fe1}} > U_{\text{Fe2}}$ for the configuration I. In the second configuration, both Fe1 and Fe2 occupy the tetrahedral sites and even if they are treated differently in our simulations, their U values came out to be same as their chemical environments are identical. The U value on Rh decreases from tetrahedral site (as in configuration I) to octahedral site (in configuration II). Slightly lower U -values observed in Fe_2RhGe as compared to Fe_2RhSi can be attributed to the reduced hybridization strength due to the ligand atom (i.e., Si or Ge) (stronger hybridization leads to larger band splittings as seen in Fe_2RhSi).

Looking at the U values on Rh (>6.6 eV), Fe1 & Fe2 (>3.9 eV) for the configuration I of Fe_2RhZ ($\text{Z}=\text{Si}, \text{Ge}$), one may argue that the estimated values are relatively large. However, these U -values are comparable to those of a similar, large moment system Co_2FeSi .⁵⁴ This system has 30 valence electrons and hence carries a net moment of $6 \mu_B$ according to the SP rule. Wurmehl *et al.* reported it to be a ferromagnet with $T_C \approx 1100$ K and an experimental moment of $6 \mu_B$.⁵⁴ It was reported that the experimentally observed moment can only be reproduced by the application of U in excess of 7.5 eV.³ They also reported that the application of $U_{\text{eff}}=U-J$ (where J is the exchange parameter) ranging between 2.5 eV to 5.0 eV on Co atom and (simultaneously) 2.4 eV to 4.8 eV on Fe atom result in a moment of $6 \mu_B$ and a gap in the minority state.⁵⁴ 3d transition elements Fe and Ni are reported to have U -values greater than 4.5 eV in FeO and NiO.⁷⁶ Therefore, the listed U values in Table II are within the expected range, for the considered elements.

Using the estimated U values from the linear response method (as tabulated in Table II) in the GGA+ U scheme,⁷⁶ electronic/magnetic properties of configurations I and II of Fe_2RhZ ($\text{Z}=\text{Si}, \text{Ge}$) were investigated. Configuration I turns out to be energetically more stable in both the cases. Figure 9 shows the spin resolved band structure and density of states for configuration I of

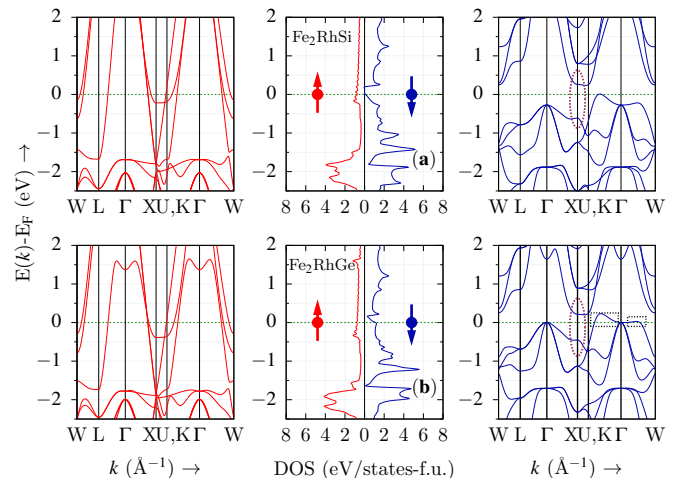


FIG. 9. Spin resolved band structure and density of states for (top) Fe_2RhSi and (bottom) Fe_2RhGe alloys using GGA+ U approach.⁷⁶ The U -values used in this calculation are listed in Table II. Dotted encircle shows the location of opening of gap. Dotted rectangle shows the location of hole pockets.

Fe_2RhZ ($\text{Z}=\text{Ge}, \text{Si}$). Interestingly, Fe_2RhSi becomes half metal whereas Fe_2RhGe remains metallic. The direct overlap of e_g conduction orbital and t_{2g} valence orbital around X -point within GGA only approach (without U) are now separated out (see the dotted encircle region in Fig. 9) due to Hubbard energies. This also changes the partially occupied conduction e_g orbitals to fully unoccupied ones by shifting them above the Fermi level in Fe_2RhZ ($\text{Z}=\text{Si}, \text{Ge}$). Fe_2RhGe does not become half metal even after applying U values because of lower band splitting energies and the presence of hole pockets in its spin down band structure. This is true even if one varies U values (on Fe1, Fe2 and Rh) in any range. On the other hand, Fe_2RhSi turns to be a half metal for any U values above 1.0 eV on Fe1, Fe2 and Rh. One can notice the hole pockets along the paths $\Gamma - K$ and $\Gamma - W$ in the spin down band structure of Fe_2RhGe (see Fig. 9). These hole pockets are responsible not only for causing large total density of states at Fermi level, as evident from experimental specific heat analysis, but also for the high temperature single magnon scattering observed in resistivity analysis. The origin of high temperature single magnon contribution to resistivity, observed for Fe_2RhSi might be due to the presence of hole like bands touching the Fermi level in spin down band structure (see Fig. 9). This approach predicts an almost constant moment of $5.00 \mu_B$ for Fe_2RhSi , unlike for Fe_2RhGe where the moment varies from $5.03 \mu_B$ to $5.25 \mu_B$ as the U values increase.

VI. CONCLUSION

Fe_2RhZ ($\text{Z}=\text{Si}, \text{Ge}$) were synthesized experimentally and found to crystallize in inverse Heusler structure.

Both the alloys are found to be ferromagnets with saturation magnetization $5.00 \mu_B$ and $5.19 \mu_B$ respectively and Curie temperature above 900 K. Resistivity measurement reveals metallic nature for both the systems. Integer moment and presence of anomalous single magnon contribution to low temperature resistivity in Fe_2RhSi indicate the possibility of being a half metal. Heat capacity analysis predicts larger density of states at Fermi level for Fe_2RhGe as compared to Fe_2RhSi and are in good agreement with the simulated values obtained using GGA+ U functional. *Ab-initio* calculations using GGA approach predicts inverse Heusler structure with ferromagnetic ordering to be energetically more favorable. The band structure obtained with GGA calculations suggest metallic behavior for both the alloys. In contrast, GGA+ U approach (with self-consistently calculated U -values) opens up a gap at/around X -point for the directly overlapped conduction e_g orbital and a valence t_{2g} orbital in spin down band structure for both the systems. Interestingly it predicts a net moment of $5.00 \mu_B$ with a half metallic nature for Fe_2RhSi . Fe_2RhGe , however, does not become half metal because of relatively low band split-

ting energies (as compared to Fe_2RhSi) arising out of a weak hybridization and presence of hole pockets along $\Gamma - K$ and $\Gamma - W$ path in the spin down band structure. Irrespective of U values (above 1.0 eV on Fe1, Fe2 and Rh) and the nature of functionals (either LDA+ U or GGA+ U), Fe_2RhSi is found to be a half metal while Fe_2RhGe remains metallic. Simulated results based on GGA+ U approach gives a very good overall agreement with experiment. Therefore, we conclude that Fe_2RhSi is a potential material for spintronics application due to its high transition temperature, half metallic nature and higher crystal stability.

VII. ACKNOWLEDGMENTS

YV and SSS acknowledge the financial support provided by IIT Bombay. YV acknowledges Dr. Durgesh Singh for his assistance in experimental measurements. AA acknowledges DST-SERB (Grant No. CRG/2019/002050) for funding to support this research.

-
- * suresh@phy.iitb.ac.in
† aftab@phy.iitb.ac.in
- ¹ F. Heusler, "Verhandlungen der deutschen physikalischen gesellschaft," (Friedr. Vieweg & Sohn, 1903) p. 219.
 - ² R. A. de Groot, F. M. Mueller, P. G. v. Engen, and K. H. J. Buschow, *Phys. Rev. Lett.* **50**, 2024 (1983).
 - ³ M. I. Katsnelson, V. Y. Irkhin, L. Chioncel, A. I. Lichtenstein, and R. A. de Groot, *Rev. Mod. Phys.* **80**, 315 (2008).
 - ⁴ X. L. Wang, *Phys. Rev. Lett.* **100**, 156404 (2008).
 - ⁵ Z. Yue, Z. Li, L. Sang, and X. Wang, *Small* **16**, 1905155 (2020).
 - ⁶ X. Wang, Z. Cheng, J. Wang, X.-L. Wang, and G. Liu, *J. Mater. Chem. C* **4**, 7176 (2016).
 - ⁷ X. Li, X. Wu, Z. Li, J. Yang, and J. G. Hou, *Nanoscale* **4**, 5680 (2012).
 - ⁸ Y. Venkateswara, S. S. Samatham, P. D. Babu, K. G. Suresh, and A. Alam, *Phys. Rev. B* **100**, 180404 (2019).
 - ⁹ J. Winterlik, G. H. Fecher, C. Felser, M. Jourdan, K. Grube, F. Hardy, H. von Löhneysen, K. L. Holman, and R. J. Cava, *Phys. Rev. B* **78**, 184506 (2008).
 - ¹⁰ S. K. Malik, A. M. Umarji, and G. K. Shenoy, *Phys. Rev. B* **31**, 6971 (1985).
 - ¹¹ S. K. Malik, A. M. Umarji, and G. K. Shenoy, *Phys. Rev. B* **34**, 3144 (1986).
 - ¹² T. Klimczuk, C. H. Wang, K. Gofryk, F. Ronning, J. Winterlik, G. H. Fecher, J.-C. Griveau, E. Colineau, C. Felser, J. D. Thompson, D. J. Safarik, and R. J. Cava, *Phys. Rev. B* **85**, 174505 (2012).
 - ¹³ L. Kautzsch, F. Mende, G. H. Fecher, J. Winterlik, and C. Felser, *Materials (Basel, Switzerland)* **12**, 2580 (2019).
 - ¹⁴ A. K. Nayak, M. Nicklas, S. Chadov, P. Khuntia, C. Shekhar, A. Kalache, M. Baenitz, Y. Skourski, V. K. Guduru, A. Puri, U. Zeitler, J. M. D. Coey, and C. Felser, *Nature Materials* **14**, 679 (2015).
 - ¹⁵ J. Sharma and K. G. Suresh, *Applied Physics Letters* **106**, 072405 (2015).
 - ¹⁶ I. D. Rodionov, Y. S. Koshkid'ko, J. Cwik, A. Quetz, S. Pandey, A. Aryala, I. S. Dubenko, S. Stadler, N. Ali, I. S. Titov, M. Blinov, V. N. Prudnikov, E. Lahderanta, I. Zakharchuk, and A. B. Granovsky, *Physics Procedia* **75**, 1353 (2015), 20th International Conference on Magnetism, ICM 2015.
 - ¹⁷ J. Liu, X. You, B. Huang, I. Batashev, M. Maschek, Y. Gong, X. Miao, F. Xu, N. van Dijk, and E. Brück, *Phys. Rev. Materials* **3**, 084409 (2019).
 - ¹⁸ A. K. Nayak, K. G. Suresh, and A. K. Nigam, *Journal of Physics D: Applied Physics* **42**, 035009 (2009).
 - ¹⁹ H. Yang, J. Yu, S. S. P. Parkin, C. Felser, C.-X. Liu, and B. Yan, *Phys. Rev. Lett.* **119**, 136401 (2017).
 - ²⁰ C. Li, J. S. Lian, and Q. Jiang, *Phys. Rev. B* **83**, 235125 (2011).
 - ²¹ A. Pham and S. Li, *Phys. Rev. B* **95**, 115124 (2017).
 - ²² C. K. Barman and A. Alam, *Phys. Rev. B* **97**, 075302 (2018).
 - ²³ W. Xiao-Tian, D. Xue-Fang, J. Hong-Ying, W. Li-Ying, L. Ran, L. Yong, L. Xiao-Chuang, Z. Xiao-Ming, W. Wen-Hong, W. Guang-Heng, and L. Liu Guo-Dong, *Acta Physica Sinica* **63**, 023101 (2014).
 - ²⁴ S.-Y. Lin, M. Chen, X.-B. Yang, Y.-J. Zhao, S.-C. Wu, C. Felser, and B. Yan, *Phys. Rev. B* **91**, 094107 (2015).
 - ²⁵ B. Yan and A. de Visser, *MRS Bulletin* **39**, 859–866 (2014).
 - ²⁶ K. Manna, Y. Sun, L. Muechler, J. Kübler, and C. Felser, *Nature Reviews Materials* **3**, 244 (2018).
 - ²⁷ Z. Wang, M. G. Vergniory, S. Kushwaha, M. Hirschberger, E. V. Chulkov, A. Ernst, N. P. Ong, R. J. Cava, and B. A. Bernevig, *Phys. Rev. Lett.* **117**, 236401 (2016).
 - ²⁸ P. J. Brown, A. P. Gandy, T. Kanomata, Y. Kusakari, A. Sheikh, K.-U. Neumann, B. Ouladdiaf, and K. R. A. Ziebeck, *Journal of Physics: Condensed Matter* **20**, 455201 (2008).

- (2008).
- ²⁹ I. Shigeta, O. Murayama, T. Hisamatsu, A. Brinkman, A. A. Golubov, Y. Tanaka, M. Ito, H. Hilgenkamp, and M. Hiroi, *Journal of Physics and Chemistry of Solids* **72**, 604 (2011), spectroscopies in Novel Superconductors 2010.
 - ³⁰ T. Kanomata, M. Kikuchi, H. Yamauci, and T. Kaneko, *Japanese Journal of Applied Physics* **32**, 292 (1993).
 - ³¹ B. Deka and A. Srinivasan, *Physica B: Condensed Matter* **476**, 118 (2015).
 - ³² K. Endo, T. Kanomata, H. Nishihara, and K. Ziebeck, *Journal of Alloys and Compounds* **510**, 1 (2012).
 - ³³ L. Bainsla, M. M. Raja, A. Nigam, and K. Suresh, *Journal of Alloys and Compounds* **651**, 631 (2015).
 - ³⁴ J. C. Suits, *Phys. Rev. B* **14**, 4131 (1976).
 - ³⁵ P. Klaer, M. Kallmayer, H. J. Elmers, L. Basit, J. Thöne, S. Chadov, and C. Felser, *Journal of Physics D: Applied Physics* **42**, 084001 (2009).
 - ³⁶ M. Yin and P. Nash, *Journal of Alloys and Compounds* **650**, 925 (2015).
 - ³⁷ M. Pugacheva and A. Jezierski, *Journal of Magnetism and Magnetic Materials* **151**, 202 (1995).
 - ³⁸ T. Kanomata, Y. Adachi, H. Nishihara, H. Fukumoto, H. Yanagihashi, O. Nashima, and H. Morita, *Journal of Alloys and Compounds* **417**, 18 (2006).
 - ³⁹ S. Berri, D. Maouche, M. Ibrir, F. Zerarga, L. Louail, and Y. Medkour, *Physica B: Condensed Matter* **418**, 58 (2013).
 - ⁴⁰ M. Emmel and G. Jakob, *Journal of Magnetism and Magnetic Materials* **381**, 360 (2015).
 - ⁴¹ K. Nikolaev, P. Kolbo, T. Pokhil, X. Peng, Y. Chen, T. Ambrose, and O. Mryasov, *Applied Physics Letters* **94**, 222501 (2009).
 - ⁴² R. Knut, P. Svedlindh, O. Mryasov, K. Gunnarsson, P. Warnicke, D. A. Arena, M. Björck, A. J. C. Dennison, A. Sahoo, S. Mukherjee, D. D. Sarma, S. Granroth, M. Gorgoi, and O. Karis, *Phys. Rev. B* **88**, 134407 (2013).
 - ⁴³ M. S. Bailey, Q. Li, E. B. Lobkovsky, D. Hinks, and J. Mitchell, *Journal of Solid State Chemistry* **181**, 30 (2008).
 - ⁴⁴ V. Alijani, J. Winterlik, G. H. Fecher, S. S. Naghavi, S. Chadov, T. Gruhn, and C. Felser, *Journal of Physics: Condensed Matter* **24**, 046001 (2012).
 - ⁴⁵ D. Rani, Enamullah, K. G. Suresh, A. K. Yadav, S. N. Jha, D. Bhattacharyya, M. R. Varma, and A. Alam, *Phys. Rev. B* **96**, 184404 (2017).
 - ⁴⁶ J. Suits, *Solid State Communications* **18**, 423 (1976).
 - ⁴⁷ Y. Venkateswara, D. Rani, K. Suresh, and A. Alam, *Journal of Magnetism and Magnetic Materials* **502**, 166536 (2020).
 - ⁴⁸ T. Graf, C. Felser, and S. S. Parkin, *Progress in Solid State Chemistry* **39**, 1 (2011).
 - ⁴⁹ I. Galanakis, P. H. Dederichs, and N. Papanikolaou, *Phys. Rev. B* **66**, 174429 (2002).
 - ⁵⁰ H. Luo, Z. Zhu, L. Ma, S. Xu, H. Liu, J. Qu, Y. Li, and G. Wu, *Journal of Physics D: Applied Physics* **40**, 7121 (2007).
 - ⁵¹ Z. Ren, S. Li, and H. Luo, *Physica B: Condensed Matter* **405**, 2840 (2010).
 - ⁵² T. Gasi, V. Ksenofontov, J. Kiss, S. Chadov, A. K. Nayak, M. Nicklas, J. Winterlik, M. Schwall, P. Klaer, P. Adler, and C. Felser, *Phys. Rev. B* **87**, 064411 (2013).
 - ⁵³ S. Wurmehl, G. H. Fecher, H. C. Kandpal, V. Ksenofontov, C. Felser, and H.-J. Lin, *Applied Physics Letters* **88**, 032503 (2006).
 - ⁵⁴ S. Wurmehl, G. H. Fecher, H. C. Kandpal, V. Ksenofontov, C. Felser, H.-J. Lin, and J. Morais, *Phys. Rev. B* **72**, 184434 (2005).
 - ⁵⁵ M. Sargolzaei, M. Richter, K. Koepf, I. Opahle, H. Eschrig, and I. Chaplygin, *Phys. Rev. B* **74**, 224410 (2006).
 - ⁵⁶ B. Balke, S. Wurmehl, G. H. Fecher, C. Felser, and J. Kübler, *Science and Technology of Advanced Materials* **9**, 014102 (2008), pMID: 27877928.
 - ⁵⁷ M. Kim, H. Lim, and J. I. Lee, *Thin Solid Films* **519**, 8419 (2011), first International Conference of the Asian Union of Magnetism Societies (ICAUMS 2010).
 - ⁵⁸ N. V. Uvarov, Y. V. Kudryavtsev, A. F. Kravets, A. Y. Vovk, R. P. Borges, M. Godinho, and V. Korenivski, *Journal of Applied Physics* **112**, 063909 (2012).
 - ⁵⁹ D. Rai, A. Shankar, Sandeep, M. Ghimire, and R. Thapa, *Physica B: Condensed Matter* **407**, 3689 (2012).
 - ⁶⁰ J.-M. Hyun and M. Kim, *Journal of the Korean Physical Society* **72**, 276 (2018).
 - ⁶¹ Enamullah, Y. Venkateswara, S. Gupta, M. R. Varma, P. Singh, K. G. Suresh, and A. Alam, *Phys. Rev. B* **92**, 224413 (2015).
 - ⁶² J. Rodriguez-Carvajal, *Physica B: Condensed Matter* **192**, 55 (1993).
 - ⁶³ K. Momma and F. Izumi, *Journal of Applied Crystallography* **44**, 1272 (2011).
 - ⁶⁴ P. Giannozzi, O. Andreussi, T. Brumme, O. Bunau, M. B. Nardelli, M. Calandra, R. Car, C. Cavazzoni, D. Ceresoli, M. Cococcioni, N. Colonna, I. Carnimeo, A. D. Corso, S. de Gironcoli, P. Delugas, R. A. D. Jr, A. Ferretti, A. Floris, G. Fratesi, G. Fugallo, R. Gebauer, U. Gerstmann, F. Giustino, T. Gorni, J. Jia, M. Kawamura, H.-Y. Ko, A. Kokalj, E. Küçükbenli, M. Lazzeri, M. Marsili, N. Marzari, F. Mauri, N. L. Nguyen, H.-V. Nguyen, A. O. de-la Roza, L. Paulatto, S. Poncè, D. Rocca, R. Sabatini, B. Santra, M. Schlipf, A. P. Seitsonen, A. Smogunov, I. Timrov, T. Thonhauser, P. Umari, N. Vast, X. Wu, and S. Baroni, *Journal of Physics: Condensed Matter* **29**, 465901 (2017).
 - ⁶⁵ P. Giannozzi, S. Baroni, N. Bonini, M. Calandra, R. Car, C. Cavazzoni, D. Ceresoli, G. L. Chiarotti, M. Cococcioni, I. Dabo, A. Dal Corso, S. de Gironcoli, S. Fabris, G. Fratesi, R. Gebauer, U. Gerstmann, C. Gougousis, A. Kokalj, M. Lazzeri, L. Martin-Samos, N. Marzari, F. Mauri, R. Mazzarello, S. Paolini, A. Pasquarello, L. Paulatto, C. Sbraccia, S. Scandolo, G. Sclauzero, A. P. Seitsonen, A. Smogunov, P. Umari, and R. M. Wentzcovitch, *Journal of Physics: Condensed Matter* **21**, 395502 (19pp) (2009).
 - ⁶⁶ G. Kresse and D. Joubert, *Phys. Rev. B* **59**, 1758 (1999).
 - ⁶⁷ A. Dal Corso, *Computational Materials Science* **95**, 337 (2014).
 - ⁶⁸ Y. Venkateswara, S. Gupta, S. S. Samatham, M. R. Varma, Enamullah, K. G. Suresh, and A. Alam, *Phys. Rev. B* **97**, 054407 (2018).
 - ⁶⁹ A. Kokalj, *Journal of Molecular Graphics and Modelling* **17**, 176 (1999).
 - ⁷⁰ N. Furukawa, *Journal of the Physical Society of Japan* **69**, 1954 (2000).
 - ⁷¹ T. Akimoto, Y. Moritomo, A. Nakamura, and N. Furukawa, *Phys. Rev. Lett.* **85**, 3914 (2000).
 - ⁷² K. Ueda and T. Moriya, *Journal of the Physical Society of Japan* **39**, 605 (1975).
 - ⁷³ M. A. Kouacou, A. A. Koua, Z. Yeo, A. Akichi, A. Tanoh, and M. Koffi, *Journal of Applied Sciences* **8**, 682 (2008).

- ⁷⁴ C. W. Tseng, C. N. Kuo, H. W. Lee, K. F. Chen, R. C. Huang, C.-M. Wei, Y. K. Kuo, and C. S. Lue, *Phys. Rev. B* **96**, 125106 (2017).
- ⁷⁵ See [Supplementary Material at \[URL\] for more details](#) .
- ⁷⁶ M. Cococcioni and S. de Gironcoli, *Phys. Rev. B* **71**, 035105 (2005).